Master Thesis
Electrical Engineering
Thesis number:

Synthetic Aperture Radar Image Quality Measurements

Subrata Kumar Das

This Thesis is presented as part of Degree of
Master of Science in Electrical Engineering

Blekinge Institute of Technology
June, 2011

Blekinge Institute of Technology
School of Engineering
Department of Electrical Engineering

Supervisor:

Viet Thuy Vu, Blekinge Institute of Technology, Karlskrona, Sweden
Prof. Paulo A. C. Marques, Instituto Superior de Engenharia de Lisboa, Lisboa, Portugal

Examiner:

Dr. Jörgen Nordberg, Blekinge Institute of Technology, Karlskrona, Sweden

This page is left blank

Abstract

Synthetic Aperture Radar (SAR) is an important tool for remote sensing now a day. SAR image quality measurements play an important role in the development of SAR image digital processing methods. The essential SAR image quality assessments are spatial resolutions, Integrated Sidelobe Ratio (ISLR) and Peak Sidelobe Ratio (PSLR). This thesis mainly focuses on the UWB SAR image quality measurements. Since the spatial resolutions depend on integration angle in UWB SAR, measurements should be performed at different integration angles for a UWB SAR system. Evaluation or comparison of the resolutions obtained with different UWB SAR systems can be based on another measurement named differential resolution measurements. For ISLR and PSLR measurements, it is seen that elliptical areas are more suitable for delimitation of mainlobe and sidelobe areas of a UWB SAR image than rectangular areas. This is proved by an investigation relied on a newly derived Impulse Response Function in SAR Imaging (IRF-SAR) instead of the widely used *sinc* function. From this investigation, we can also see that a factor of 2.5 is sufficient to represent the spread of mainlobe in both azimuth and range direction.

In this work, we use simulated UWB-low frequency CARABAS-II data. The simulations are performed in Matlab. In spite of the main drawback in computational cost, Global Backprojection (GBP) algorithm is still selected for UWB SAR image formation due to its time-domain characteristics such as extreme range migration handling, manageable motion compensation.

Key Words: SAR, UWB SAR, spatial resolution, differential resolution, ISLR, PSLR, sinc function, IRF-SAR.

This page is left blank

Acknowledgements

I would like to express my deepest gratitude to my supervisors Tekn. Lic. Viet Thuy Vu and Prof. Dr. Paulo A. C. Marques and to my examiner Dr. Jörgen Nordberg for continuously supporting me in the work with this thesis. Their valuable discussions, constructive advice and suggestions during the execution and writing of this thesis were very invaluable. I was very fortunate to have Viet Thuy Vu and Paulo A. C. Marques as a continuous resource for my work. Perhaps more importantly, they have provided me a perfect example by establishing a productive and enjoyable advisor-student relationship. I am very much grateful to Viet Thuy Vu for giving me the lab facilities in Ronneby.

It is my pleasure to thanks my friends who relentlessly supported me in my ways that I cannot fully express in the limited available space.

A special thanks to my wife for encouragement and immense mental support that helped me much to complete this thesis. I am grateful to god for his blessings, giving strength in all ways, keeping me safe and sound. Though him everything is possible that's why I am forwarding my thesis.

Subrata Kumar Das

June 2011

Email address:subrata_1970@yahoo.com

This page is left blank

Table of Contents

Abstract……...….I
Acknowledgements…….…….III
Table of Contents…….....……...V
List of Figures…….…….……VII
List of Tables…….…….....IX

CHAPTER 1 …….……..1
Introduction…….……..……..1
1.1 Introduction…….…….....1
1.2 Thesis Outline……...….....3

CHAPTER 2.....4
SAR and UWB SAR……...4
2.1 Radar…….....4
2.2 SAR……..….....5
2.2.1 SAR History…….....….....5
2.2.2 SAR Acquisition Mode and Techniques…….…….....6
2.2.3 SAR Resolution……..……...7
2.2.4 Pulse Compression…….……...…….....9
2.3 UWB SAR…….....10

CHAPTER 3……..……...12
Imaging Algorithms and GBP Algorithms…….……..12
3.1 Frequency-Domain Algorithms…….……..……12
3.1.1 Range Doppler Algorithm…….…….……12
3.1.2 Range Migration Algorithm…….……....……..12
3.1.3 Chirp Scaling Algorithm……....13
3.2 Time Domain Algorithms……...…...13
3.2.1 Global Backprojection Algorithm…….……...……14

CHAPTER 4…….…….…...16
Impulse Response Function for SAR imaging…….….16
4.1 Impulse Response Function……..…….....16

4.2 IRF-SAR Measurements……..……...16
4.2.1 The Locus of the First Nulls Determination…….……17
4.2.2 The dimensions of Mainlobe and Sidelobe areas…….……..…....18

CHAPTER 5…….21
UWB SAR Image Quality Measurements ……..……..21
5.1 Spatial Resolution…….…….....21
5.2 Differential Resolution…….……...…..21
5.3 Integrated Sidelobe Ratio (ISLR)…….…….....22
5.4 Peak Sidelobe Raio (PSLR)……..…….....22

CHAPTER 6…….……23
UWB SAR Image Quality Measurement Results…….23
6.1 Spatial resolution and differential resolution measurements ……..…..23
6.2 ISLR and PSLR measurements…….……28

CHAPTER 7…….……31
Conclusions and Recommendations…….31

References…….....32

List of Figures

Fig 2.1: Basic block diagram of typical radar system……...……..4
Fig 2.2: Spaceborne and airborne SAR system……...……7
Fig 2.3: SAR geometry……..……8
Fig 2.4: Cross- range and range resolution of SAR…….…...9
Fig 2.5: Match filtering of received echo……..…….…...10
Fig 2.6: Power spectral density of NB and UWB signals.…….…..…..11
Fig 3.1: RD processing…….…….……13
Fig 3.2: (a) SAR system geometry and (b) SAR signal history…….…...14
Fig 4.1: The locus of the first nulls…….…..18
Fig 4.2: IRF-SAR in azimuth direction…….....19
Fig 4.3: IRF-SAR in range direction…….…....19
Fig. 6.1: (a) A point target is imaged by an UWB SAR system with an integration angle of 65 degrees, (b) The extracted range vector from the peak, (c) The extracted azimuth vector from the peak……24
Fig 6.2: Plot of the spatial resolutions measurements…….…….….25
Fig 6.3: Plot of the differential resolution calculations……..…27
Fig. 6.4: Mainlobe area delimitation at 65 degrees……...28
Fig. 6.5: Mainlobe plus sidelobe area delimitation at 65 degrees…….28
Fig 6.6: ISLR and PSLR at different integration angles……...30

This page is left blank

List of Tables

Table 2.1: Different UWB SAR systems……..……..…11
Table 4.1: FNBW with different values of φ_t from 0 to 90 degrees……....17
Table 4.2: Values of HPBW and FNBW in azimuth direction…….18
Table 4.3: Values of HPBW and FNBW at range direction…….19
Table 6.1: CARABAS-II parameters……23
Table 6.2: Spatial resolutions in range and azimuth measured at different integration angles……....25
Table 6.3: Differential resolutions in range and azimuth calculated at different integration angles……26
Table 6.4: ISLR and PSLR measured at different integration angles……...29

This page is left blank

CHAPTER 1

Introduction

1.1 Introduction

Radar is a sensor that transmits and receives electromagnetic energy. Since it utilizes its own radio energy to detect and track the target, radar operates equally well day or night and is not significantly affected by fog, cloud, or precipitation. It has long been used for military and non-military purposes in a wide variety of applications such as imaging, guidance, remote sensing, and global positioning [1]. Real aperture imaging radar and side looking airborne radar (SLAR) have been developed to produce better quality images for military use. However, the image formed by SLAR is usually poor in azimuth resolution.

The synthetic aperture radar principle has been discovered in the early 50th. Since then, a rapid development took place all over the world and a couple of air and space -borne systems are operational today. Progress made in technology and digital signal processing lead to very flexible systems useful for military and civilian applications [2]. Synthetic aperture radar (SAR) are imaging radars that by taking advantage of the motion of the radar and utilizing sophisticated signal processing, the limitations imposed by physical and electrical constraints are improved. SAR is able to extract two-dimensional images of an area of a surface from the received signals with very high resolution [3]. In SAR, forward motion of actual antenna is used to "synthesize" a long antenna.

A SAR system utilizing large fractional bandwidth signal and wide antenna beamwidth is interpreted as ultrawideband ultrawidebeam (UWB) SAR. Such system has shown the ability to image large ground scenes with high resolution. In this thesis, the simulated CARABAS-II data is used. In reality, CARABAS-II is an airborne UWB low frequency SAR system, operates in the VHF band 20-90 Mhz and utilizes dipole antennas with the beamwidth of more than 90° [4]. UWB SAR imaging faces inherent challenges such as the choice of processing algorithm, integration angle, apodization, motion compensation and radio frequency interference (RFI) [5]. RFI is a major problem for low-frequency SAR systems operating in the VHF/UHF-band, because the spectrum is already used extensively by other services such as television, mobile communication, radio and cellular phones. The interference power often exceeds receiver noise by many dB, becoming the limiting factor as

system sensitivity and severely degrades image quality [6]. The choice of imaging algorithm is an important issue for UWB SAR as it requires extreme range migration and large motion compensation. Between frequency-domain algorithm and time-domain algorithm, frequency domain is more efficient due to reduction of processing load and it can produce good image quality for non UWB SAR. For UWB SAR systems, it does not provide good image quality because of insufficient motion compensation. The global backprojection (GBP) algorithm is the root of all time-domain algorithms which was first introduced in 1980's. This algorithm provides high quality of SAR images by linear and direct transformation of radar echoes. Frequency-domain algorithms cannot perform good motion compensation but GBP can do it automatically for nonlinear aperture. The image quality obtained by this algorithm is the same as obtained for linear aperture. The GBP algorithm can handle extreme range migration and provides manageable motion compensation, which make it convenient use in UWB SAR image formation. Another unique feature of GBP is that it can illuminate scene size unlimited. But this unlimited illumination matter is related to the antenna beamwidth, integration time, flight altitude, radiated power, pulse repetition frequency (PRF) of SAR system. In GBP, the number of operations to process an $N_x \times N_r$ SAR image where N_x denotes the number of image pixels in the azimuth and N_r denotes the number of image pixels in the range with N_a aperture positions is proportional to $N_x \times N_r \times N_a$.

The main drawback of this algorithm is high computational cost as the computational load increases proportionally with the size of the image and the number of aperture position. In NB SAR, there exists only orthogonal sidelobes but in UWB SAR both orthogonal and non-orthogonal sidelobes are present. For narrowband imaging, two-dimensional (2-D) *sinc* function is widely used and for UWB SAR imaging a new impulse response function (IRF-SAR) is used. As NB SAR systems utilize small fractional bandwidth and narrow antenna beamwidth so, rectangular delimitations of the mainlobe and sidelobe areas can be used. But UWB SAR systems utilize large fractional bandwidth and wide antenna beamwidth, so elliptical instead of rectangular delimitation of the mainlobe and sidelobe areas should be used as the locus of first nulls of the mainlobe close to an ellipse [4].

SAR image quality measurements are usually based on point target analysis. The most significant parameters for image quality measurements are spatial resolutions. It can be experimentally measured on images containing strongly reflecting scatters such as corner reflectors [4]. Spatial resolution in azimuth Δx and range Δr are defined by -3 dB beamwidth of the mainlobe. Other image quality parameters such as integrated sidelobe ratio

(ISLR) and peak sidelobe ratio (PSLR) can also evaluated from a point target. The former can be defined as the ratio of the power in the main peak to the total power in all the side lobes. The later is defined as the ratio of the peak intensity of the most prominent sidelobe to the peak intensity of the mainlobe.

Some NB SAR image quality measurements such as ISLR and PSLR do not work for UWB SAR systems because rectangles are used to delimit the mainlobe and sidelobe areas. Measurements with currently used definitions on SAR image quality for UWB SAR may therefore be inexact; especially the measurements based on integrated energy. These measurements should also be performed at different integration angles since different azimuth focusing obtained at different integration angles results in different spatial resolution in azimuth and therefore different ISLR and PSLR [4].

In the thesis main focus are the SAR image quality measurements such as spatial resolutions in azimuth and range, ISLR, PSLR, and differential resolution. The work is started with a studying a basic time-domain algorithm GBP, implementing it in matlab, and then performing UWB SAR image quality measurements.

1.2 Thesis Outline

The thesis comprised of the following chapters.

Chapter 2 introduces SAR and UWB SAR.

Chapter 3 summaries different SAR imaging algorithms and also presents GPB algorithm.

Chapter 4 presents the IRF-SAR functions.

Chapter 5 discusses SAR image quality in general and UWB SAR image quality in particular.

Chapter 6 provides the experimental results.

Chapter 7 presents the conclusion with possible future work.

CHAPTER 2

SAR and UWB SAR

This chapter introduces the background information on SAR, UWB SAR and the key parameters used later in the thesis.

2.1 Radar

Radar has long been used for military and non-military purposes in a wide variety of applications such as imaging, guidance, remote sensing and global positioning. The term Radar is an acronym derived from radio detection and ranging. Today radar is usually defined as active electromagnetic surveillance.

Basically, the function of radar is to transmit a burst of electromagnetic energy necessary to allow detection of targets and intercept the energy by its receiver. When radio waves strike an object, some portion is reflected, and some of this reflected energy is returned to the radar set, where it is detected. The location and other information about these reflected objects, length, can be determined by the reflected energy. Actually, it works like a flash camera but at radio frequency. A basic radar system consists of transmitter, switch, antenna, receiver, and data recorder. The transmitter transmits a high power pulse to a switch at radio wavelengths. The switch directs the high power pulse to antenna and returns echo to receiver. The radar antenna illuminates the target with a microwave signal, which is then reflected, and a receiving device collects returned echoes. The returned echo signal is converted to digital number by the receiver and the data recorder stores data values for later processing and display [7]. Fig. 2.1 shows the basic block diagram of a radar system.

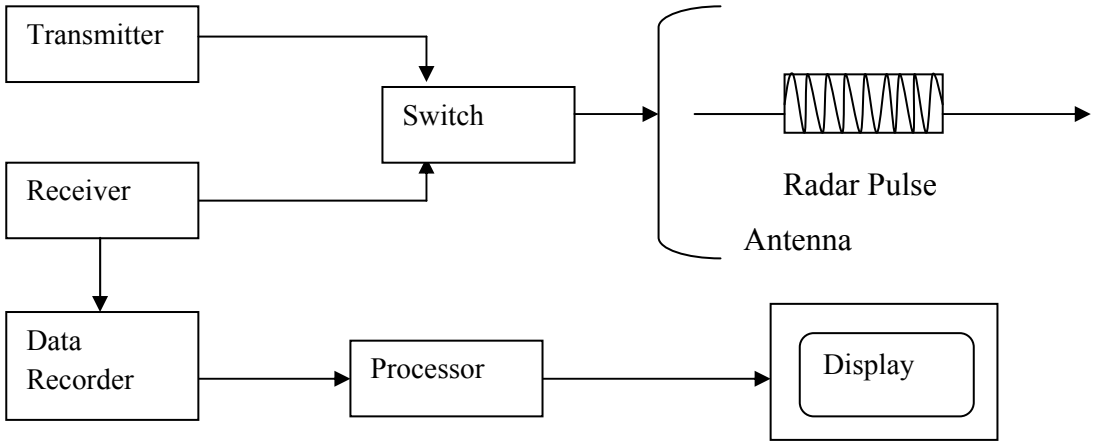

Fig. 2.1: Basic block diagram of typical radar system.

The radar equation is a mathematical analysis that can be used to predict the maximum range at which the radar would be able to detect a particular target. The radar equation for a monostatic radar system can be written as

$$P_r = \frac{P_t G^2 \lambda^2 \sigma}{(4\pi)^3 R^4} \tag{2.1}$$

where P_r is the power received at the antenna power received at the antenna, P_t is the power radiated by the antenna, G is antenna gain, R is the distance from radar to the target, λ is the operating wavelength, σ is the radar target cross section. Thus, the power returned from a target to antenna as an imaging radar system is directly proportional to the transmitted power, the area of the resolution cell and is inversely related to the fourth power of range.

2.2 SAR

SAR is an active microwave sensing system which has widely used ground imaging radars. SAR systems are mounted on an airplane or satellite which has the ability to effectively collect data in severe conditions like rain, cloud and darkness. This is the main reason which gives SAR systems such diverse applications in geosciences, remote sensing, surveillance, and reconnaissance. SAR produces a 2-D image from long distances. One dimension of the image is called range or cross track range. The range resolution is the function of transmitted pulse width i.e. narrow pulse yields fine range resolution. The other dimension of the image is azimuth or along track range and is perpendicular to cross track. Azimuth resolution can be defined as the minimum distance on the ground in the direction parallel to the flight path of the aircraft at which two targets can be separately imaged. In order to improve fine azimuth resolution, a physically long antenna is needed to focus the transmitted energy into a sharp beam. For high resolution SAR image, a fine azimuth resolution is necessary. But constructing an antenna of several hundred meters is quite difficult task. In reality, SAR is based on the principle of generation of an effective long antenna by signal processing means rather than by the actual use of long physical antenna.

2.2.1 SAR History

Development of radar as a tool for ship and aircraft detection was started during 1920's. Engineers begin to attach the radar antenna to the fuselage of aircraft in the late 1930's and this lead to a new idea of SLAR in the field of radar imaging. The first imaging radar, developed during World War II, used the B-scan which produced an image in a rectangular format. However, the image formed by SLAR is poor in azimuth resolution. In June 1950,

Carl Wiley described the use of Doppler frequency analysis to improve radar image resolution. The technique was originally called Doppler beam sharpening, but today is known as SAR [8].

2.2.2 SAR Acquisition Mode and Techniques

Depending upon the system configuration, SAR sensor can acquire data in three different modes: stripmap, scan, and spotlight. They are described as bellows.

Stripmap mode: When operating as a stripmap SAR, the radar antenna pointing direction is fixed with respect to the platform flight track and the illumination footprint covers a strip on the ground as the platform moves. The finest azimuth resolution is independent of the sensor–target range and is equal to half of the physical antenna length in the azimuth direction.

Scan mode: While operating as a ScanSAR, the sensor antenna beam is periodically stepped in range to neighbor swaths referred to as sub-swaths. As a result the overall dimension of range swath is increased for each target. In the ScanSAR mode, the full antenna synthesis is not possible and the range swath width increases at the expense of the azimuth resolution.

Spotlight mode: When operating as a spotlight SAR, the sensor steer its antenna beam to continuously illuminate the terrain patch being imaged. In this mode, finer azimuth resolution is achieved than in the stripmap mode using the same physical antenna. The spotlight mode offers efficient imaging of multiple smaller scenes while the stripmap mode images a long strip of terrain [9].

Basically, SAR systems can be divided into two groups based on the operating platforms. They are described as bellows.

Airborne SAR: These systems are operating on variety of aircrafts. In airborne systems, incidence angles for wide swath coverage vary considerably across the swath and typical altitudes 5–10 km.

Spaceborne SAR: These systems are operating on satellite or space shuttle platforms. In spaceborne systems, incidence angles across the same swath vary only slightly and typical altitudes 250–800 km. Fig. 2.2 will give better understanding of the Spaceborne and airborne SAR system.

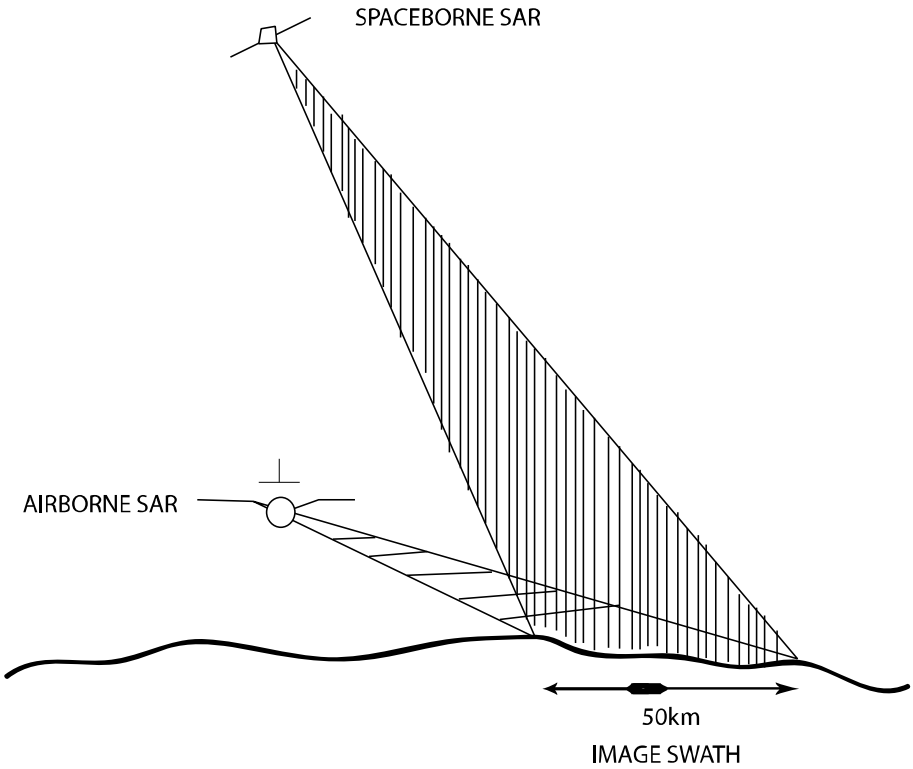

Fig. 2.2: Spaceborne and airborne SAR system.

2.2.3 SAR Resolution

For two dimensional imaging, resolution is divided into two components, range and cross range (azimuth).

Range Resolution

Range resolution is defined as the minimum distance along the radar line of sight between two scatters inside the footprint at which they can still be detected individually. The roundtrip propagation delay is shown in the following equation.

$$t = \frac{2R}{c} \tag{2.2}$$

where R is the distance, and c is the propagation velocity. Then a pulse of duration τ corresponds to a range increment [10] is

$$\Delta R = \frac{c\tau}{2} \tag{2.3}$$

For improving range resolution, the pulse duration should be decreased but this would reduce the average transmitted power and degrade the signal to noise ratio (SNR). So the peak power needs to be increased but there are some constraints. Fig. 2.3 gives better understanding of the SAR geometry.

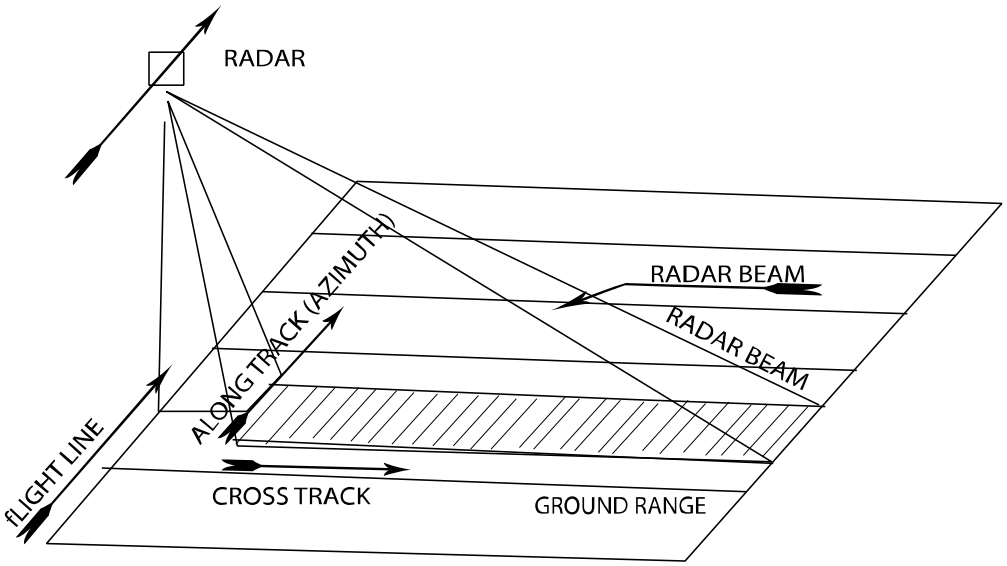

Fig. 2.3: SAR geometry.

Cross-range Resolution

Cross-range resolution is the minimum distance on the ground in the direction parallel to the flight path of the aircraft at which two targets can be separately imaged. Synthetic aperture processing methods attempt to enhance cross-range with the help of advanced digital signal processing to synthesize a large antenna aperture so that it is comparable to range resolution. For a physical antenna with an aperture D, operating at an wavelength λ, the cross–range resolution is given by

$$\Delta X = R\theta_B = \frac{\lambda R}{D} \tag{2.4}$$

where R is the range between the center of the footprint, and the antenna θ_B is the azimuth –3 dB beamwidth. From the equation, it is seen that resolution degrades with the increasing target distance. Because of wavefront spreading, illumination is increased with distance. As a result, target reflections within the area are received at the same time and cannot be resolved. There are two ways to improve the cross-range resolution. One approach is to adjust the physical parameters and the antenna itself because narrower beamwidth enhances resolution. But the mechanical problems involved in constructing an antenna with a surface precision accurate to within a fraction of wavelength, and the difficulty in maintaining that level of precision in an operational environment, make it difficult to attain values of D/λ greater than a few hundred aperture [8]. Fig. 2.4 illustrates the definitions of the cross-range and range resolutions of a SAR system.

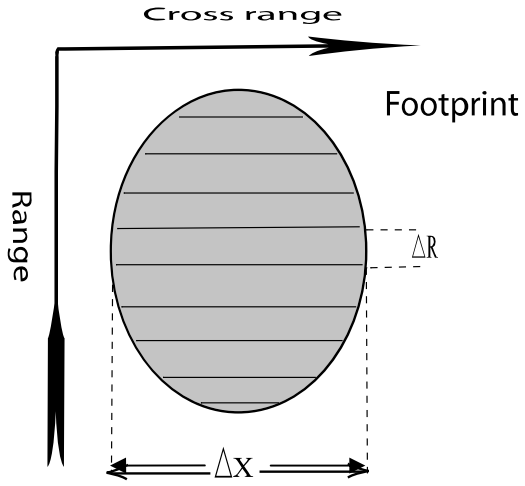

Fig. 2.4: Cross-range and range resolution of SAR [3].

Another approach to improve azimuth resolution is to introduce the concept of a synthetic array. The main concept of this approach is that a physical antenna becomes one element of synthetic array and data is collected sequentially as the antenna moves to each point within the array. An effective aperture is synthesized by advance signal processing the data which in turn increases the range resolution without unrealistically large antenna apertures.

The increase in effective aperture size exactly cancels the beamwidth range dependence that limits the real aperture and then cross- range resolution is defined by the following equation

$$\Delta X = \frac{D}{2} \tag{2.5}$$

So cross-range resolution becomes range independent.

2.2.4 Pulse Compression

Pulse compression is a technique using a matched filter to compress the energy in a signal into a narrow pulse. This technique uses in SAR to shorten the transmitted pulse τ_p. The main concept of pulse compression is to keep the pulse duration the same but divide it into shorter pulse $\delta\tau_p$, detectable by the signal processor. In most radar systems, only a single frequency carrier signal is used and it is modulated with a rectangular pulse of duration τ_p seconds. The bandwidth of this modulated signal is shown in the following equation.

$$B = \frac{1}{\tau_P} \tag{2.6}$$

But if the single carrier frequency is divided into *N* successive steps of Δf Hz and modulated with the same rectangular pulse then the waveform bandwidth can be shown as

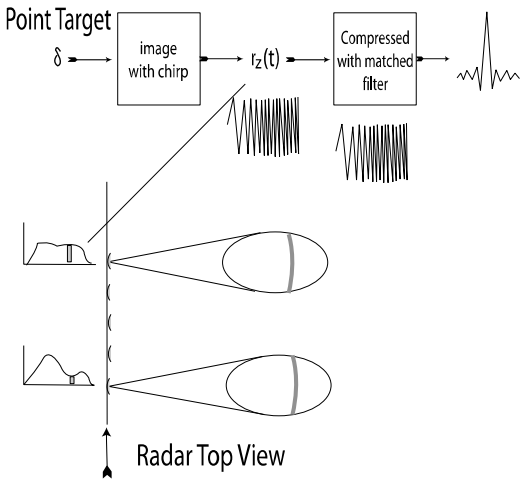

Fig 2.5: Match filtering of received echo [11].

$$B = (N-1)\Delta f \gg \frac{1}{\tau_p} \tag{2.7}$$

Then the effective pulse duration is 1/*B*. Actually, step frequencies are not used for SAR but the linear frequency modulation (LFM) or chirp signal is used in SAR. The utility of chirp waveform in imaging radar is that the duration of this chirp signal can be long compared to that of the CW (Continuous Waveform) burst pulse and yet the result is the same effective bandwidth. Fig. 2.5 shows the waveform of a pulse modulated LFM signal [3]. The waveform equation of an LFM signal can be defined as follows

$$s(t) = \text{Re}\{s(t)\} = \cos\left\{2\pi\left(f_c t + \frac{\kappa t^2}{2}\right)\right\} \tag{2.8}$$

where $-\frac{\tau_p}{2} \leq t \leq \frac{\tau_p}{2}$, κ is the chirp rate of the waveform, and f_c is the center frequency of transmitted waveform. The bandwidth of an LFM signal is therefore given by the following equation

$$B = \kappa t \tag{2.9}$$

and the instantaneous frequency, $f(t)$, of an LFM signal is given as

$$f(t) = f_c + kt \tag{2.10}$$

2.3 UWB SAR

An UWB SAR system transmits UWB signal and utilizes a wide antenna beamwidth for better resolution and more spectral information of target reflectivity. It is a new tool that shown effectiveness for the detection of targets buried underground using longer wavelength UWB signals for high resolution allows the radar to penetrate foliage and camouflage [12]. Some UWB SAR systems are shown in the Table 2.1.

Table 2.1: Different UWB SAR systems

Name of the system	Frequency band	Frequency
CARABAS-II	Lower VHF band	20-90 MHz
LORA	VHF/UHF	200-800 MHz
P-3	VHF/UHF	215-900 MHz
PAMIR	X-Band	12.5-8.0 GHz
BoomSAR	VHF/UHF	50-1200 MHz

While there is still no definition of the antenna beamwidth connected to the UWB SAR, the common definition of UWB signal is either given by [13]

$$f_r = \frac{f_{max} - f_{min}}{f_c} \geq 25\% \tag{2.11}$$

or

$$B > 1.5 \text{ GHz} \tag{2.12}$$

where f_{min} is the minimum frequency, f_c is the center, and f_{max} is the maximum frequency of the signal. Federal Communications Commission (FCC) proposed another definition of UWB in 2002 either by

$$f_r = \frac{f_{max} - f_{min}}{f_c} \geq 20\% \tag{2.13}$$

or

$$B > 500 \text{ MHz} \tag{2.14}$$

Fig. 2.6 sketches the power spectral density of the NB and UWB signals.

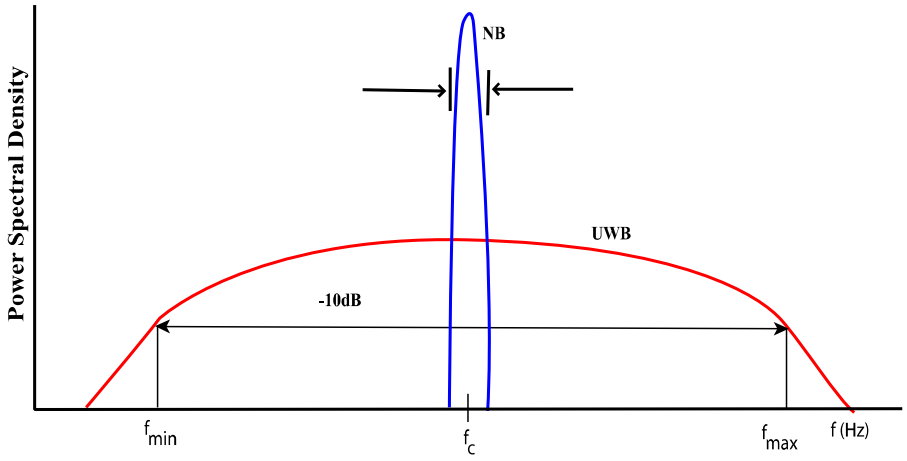

Fig. 2.6: Power spectral density of NB and UWB signals.

CHAPTER 3

Imaging Algorithms and GBP Algorithms

Digital SAR data processing, which is an active field of research now a day, plays an important role in SAR images. In comparison with optical images, SAR data have to be preprocessed in order to obtain an image. The Range Doppler (RD) [14], algorithm is the first computer based SAR image processing algorithms introduced in 1970's. The image processing algorithms involved with SAR are basically divided into two major groups: time-domain algorithm and frequency- domain algorithm. The main consideration in defining groups is to first identify what domain the processing is carried out. Regardless of the domain, all are employed to improve azimuth (cross-range) resolution. Both algorithms have some merits and demerits.

3.1 Frequency-Domain Algorithms

RD, Range Migration (RM), and Chirp Scaling (CS) are mostly used frequency-domain algorithms. The main advantage of the frequency domain techniques is the computational efficiency. The algorithms are only valid for the linear cases where the flight trajectory is straight and the speed is constant. The algorithms are still usable since the flying trajectory can be considered linear in short distances.

3.1.1 Range Doppler Algorithm

Range Doppler algorithm is the most common frequency domain algorithm employed in most of the SAR processing system. It is a two-dimensional correlating procedure. The two dimensions of the correlation processing are realized as two one-dimensional matched filter operations namely range compression and azimuth compression. The first matched filtering operates on the single pulse radar returns and the second matched filtering operation operates on the Doppler signal. Fig. 3.1 shows the block diagram of the SAR processing with RD [7].

3.1.2 Range Migration Algorithm

The RM algorithm is also known as $\omega - k$ algorithm. This algorithm introduces a new coordinate in the wave number domain so that the signal gets a linear phase in the new coordinate systems. The substitution is done by [2]

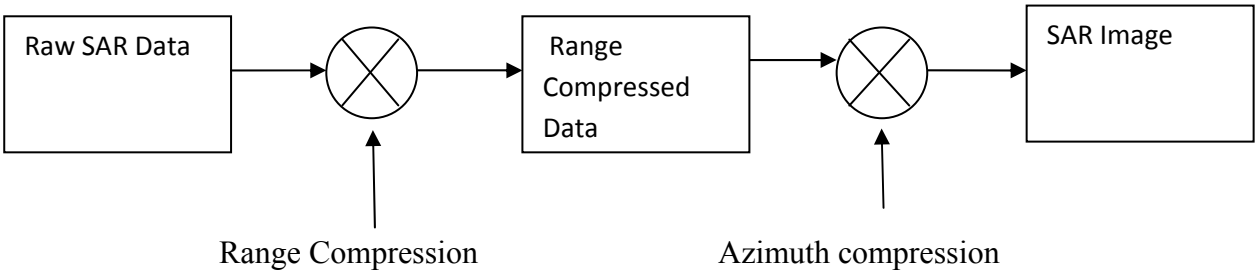

Fig. 3.1: RD processing.

$$k_\rho = \sqrt{k_r^2 - k_x^2} \tag{3.1}$$

where k_ρ is the wave number in slant range, k_r is the range wave number, and k_x is the azimuth wave numbers. This substitution enables a resampling in the new coordinate k_ρ.

In RM, the received echo is transformed into a finite number of evenly-spaced points in the frequency wave number domain via two-dimensional FFTs. This algorithm requires the so-called Stolt interpolation to calculate the new samples and it offers high SAR image quality at fine resolution.

3.1.3 Chirp Scaling Algorithm

The CS algorithm is a new method of SAR processing which avoids interpolation but performs range cell migration correction accurately. It is also known as the differential range deramp or DRD algorithm [15]. This algorithm requires only complex multipliers and Fourier Transform (FT) to implement, is inherently phase preserving and is suitable for spaceborne SAR application. The only demerits of this algorithm is that it requires large amount of memory to process the raw SAR data and this algorithm is limited to radar systems that use LFM chirps as their transmit modulation. The extended chirp scaling, an improved version of this algorithm has been developed to allow the accurate processing of airborne SAR and is able to compensate motion errors. A geometric scaling of data in range and/or azimuth directions can be achieved without interpolation. The CS algorithm and the extended version are not valid for VHF systems and also for large squint angles and high range bandwidths.

3.2 Time Domain Algorithms

Among time-domain algorithms, the Gobal Backprojection algorithm (GBP) is the root of all time-domain algorithms which was first introduced in 1980's. This algorithm provides high quality of SAR images by linear and direct transformation of radar echoes. Other fast time-

domain algorithms are Local Backprojection (LBP) and Fast Factorized Backprojection (FFBP) which are introduced to overcome the heavy computational load problem of the GBP.

3.2.1 Global Backprojection Algorithm

The main idea of backprojection is a match-filter implementation of time-domain correlation. Actually, backprojection is an image reconstruction algorithm that is used in a number of applications, including SAR and Computer Axial Tomography in medical imaging [16]. It provides a method for implementing an image from the data that is collected by the transceiver. Data collected at each aperture position is a function of round-trip delay time and it is correlated. Backprojection coherently sums the sampled SAR returns for each array element (pixel) of the image map. In GBP, the backprojection can be expressed by the following integral

$$h(x_0, r_0) = \int_{-\frac{l}{2}}^{+\frac{l}{2}} g(x, r)dx \tag{3.2}$$

where $h(x_0, r_0)$ is the backprojected signal, l is the aperture length, x is the platform positions in the flight track, and $g(x, r)$ is the range compressed data of the stationary point target. For straight flight track along the *x*-axis, the range r to the point (x_0, r_0) can be shown by the following hyperbolic function [4]

$$r = \sqrt{(x - x_0)^2 + {r_0}^2} \tag{3.3}$$

Fig. 3.2 illustrates the SAR system geometry and shows SAR signal history.

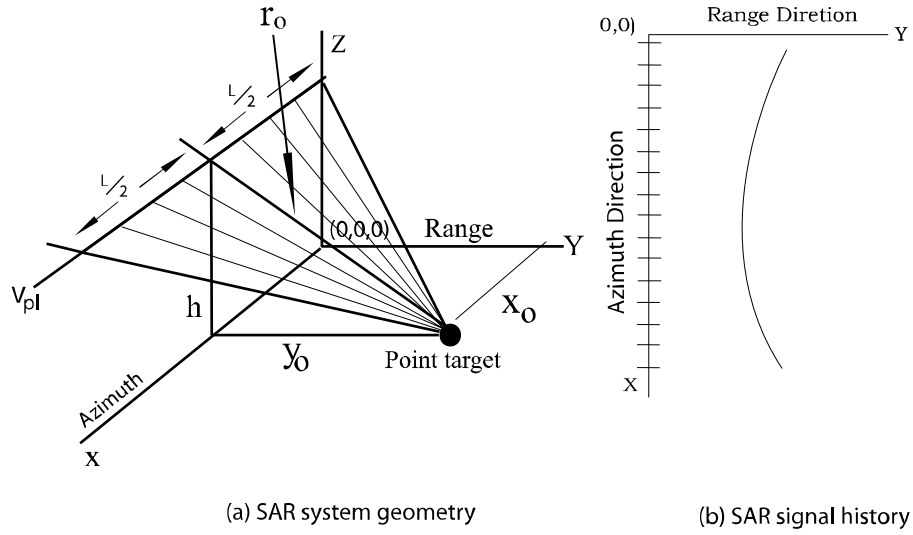

Fig. 3.2: (a) SAR system geometry and (b) SAR signal history.

Basically, this algorithm provides extreme range migration and motion compensation, which make it convenient use in UWB SAR image formation. All other time-domain algorithm like LBP and FFBP are developed from this algorithm. Another unique feature of GBP is that it can illuminate scene size unlimited. However, this unlimited illumination matter is related with the antenna beamwidth, integration time, flight altitude, radiated power, and Pulse Repetition Frequency (PRF) of a SAR system [5].

Considering an $N_x \times N_r$ SAR image where N_x denotes the number of image pixels in the azimuth and N_r the number of image pixels in the range direction. We also assume that the image is formed from the data of N_a aperture positions. The number of operations required by GBP will be proportional to $N_a \times N_x \times N_r$. This clearly shows the high computational cost of GBP because the computational load increases proportionally with the length of the aperture and the size of the image and therefore the main drawback of this algorithm.

CHAPTER 4

Impulse Response Function for SAR imaging

In this chapter a newly derived IRF-SAR function for UWB SAR imaging is discussed. This function is important for delimitations of mainlobe and sidelobe areas of SAR image. Then the locus of the first nulls is determined.

4.1 Impulse Response Function

The two-dimensional *sinc* function is normally used for Impulse Response Function in SAR imaging (IRF-SAR). As it deals with rectangular approximation, NB SAR systems only work with it smoothly. But *sinc* function does not give the accurate result for UWB SAR. For UWB SAR systems which deal with large integration angles and fractional bandwidth, a new IRF-SAR is needed. The new IRF-SAR is defined by the following equations [17].

$$h(\rho, \varphi_t, B_r, \phi_0) = \frac{e^{-i\varphi_t}}{\rho}\left[\phi_0 \sum_{n=-\infty}^{+\infty} \frac{i^n h_{1,n-1}(\rho, B_r)}{\mathrm{e}^{i(n-1)\varphi_t}} \mathrm{sinc}\left(n\frac{\phi_0}{2}\right)\right] + \frac{e^{-i\varphi_t}}{x} h_2(\rho, \varphi_t, B_r, \phi_0) \tag{4.1}$$

where

$$h_{1,n-1}(\rho, B_r) = -\left(1+\frac{B_r}{2}\right) J_{n-1}\left[\rho\left(1+\frac{B_{-r}}{2}\right)\right] + \left(1-\frac{B_r}{2}\right) J_{n-1}\left[\rho\left(1-\frac{B_r}{2}\right)\right] \tag{4.2}$$

$$h_2(\rho, \varphi_t, B_r, \phi_0) = B_r \mathrm{sinc}\left[\frac{B_r}{2}\rho\cos\left(\frac{\phi_0}{2}-\varphi_t\right)\right] \mathrm{e}^{i\rho\cos\left(\frac{\phi_0}{2}-\varphi_t\right)+i\frac{\phi_0}{2}} - B_r \mathrm{sinc}\left[\frac{B_r}{2}\rho\cos\left(\frac{\phi_0}{2}+\varphi_t\right)\right] \mathrm{e}^{i\rho\cos\left(\frac{\phi_0}{2}+\varphi_t\right)-i\frac{\phi_0}{2}} \tag{4.3}$$

Equation (4.1) allows us to find the locus of the first nulls, which can be further used to delimit the mainlobe area, broadening factor of the mainlobe, and also those of sidelobe area.

4.2 IRF-SAR Measurements

As mentioned earlier in this chapter that the commonly used *sinc* function is not suitable for UWB SAR systems. To find the shapes of mainlobe and sidelobe areas as well as the dimensions of these areas, IRF-SAR defined by (4.1) will be used.

Table 4.1: FNBW with different values of φ_t from 0 to 90 degrees.

φ_t	FNBW	φ_t	FNBW	φ_t	FNBW	φ_t	FNBW
0	12.8	23	10.2	46	8	69	7.0
1	12.8	24	10.2	47	8	70	7.0
2	12.8	25	9.8	48	8	71	7.0
3	12.6	26	9.8	49	7.8	72	7.0
4	12.6	27	9.6	50	7.8	73	7.0
5	12.6	28	9.6	51	7.8	74	7.0
6	12.2	29	9.4	52	7.8	75	7.0
7	12.2	30	9.4	53	7.8	76	7.0
8	12.2	31	9.4	54	7.4	77	7.0
9	12	32	9.0	55	7.4	78	7.0
10	12	33	9.0	56	7.4	79	6.6
11	11.8	34	9.0	57	7.4	80	6.6
12	11.8	35	8.8	58	7.4	81	6.6
13	11.6	36	8.8	59	7.2	82	6.6
14	11.2	37	8.8	60	7.2	83	6.6
15	11.2	38	8.6	61	7.2	84	6.6
16	11.0	39	8.6	62	7.2	85	6.6
17	11.0	40	8.6	63	7.2	86	6.6
18	10.6	41	8.2	64	7.2	87	6.6
19	10.6	42	8.2	65	7.2	88	6.6
20	10.4	43	8.2	66	7.2	89	6.6
21	10.4	44	8.2	67	7.0	90	6.6
22	10.2	45	8.0	68	7.0		

4.2.1 The Locus of the First Nulls Determination

It is necessary to find the locus of the first nulls to define the shape of the mainlobe. The shape of the mainlobe area can be defined by investigating the Fist Null Beamwidth (FNBW) with different values of φ_t from 0 to 90 degrees. Due to symmetry of IRF-SAR, other FNBW corresponding to the values of φ_t from 90 to 360 degrees can be inferred. FNBW of IRF-SAR with different values of φ_t are listed in Table 4.1. The factional bandwidth and integration angle is selected by $B_r = 1.2$ and $\phi_0 = 110^{\mathrm{o}}$ which are parameters of a UWB SAR system.

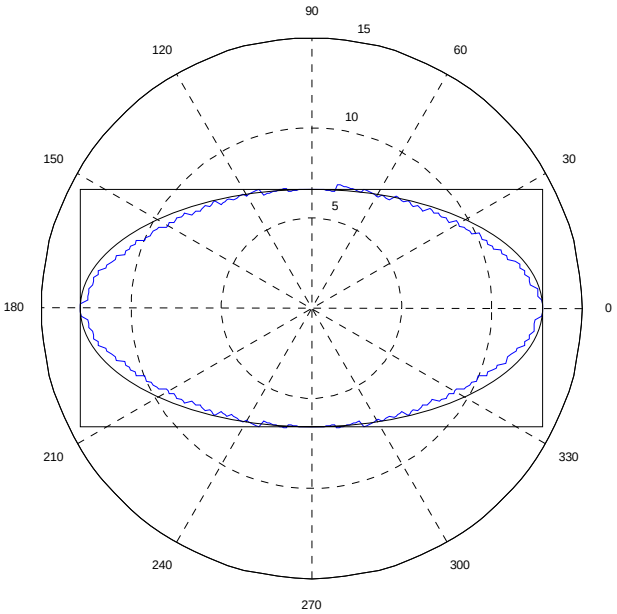

Fig 4.1: The locus of the first nulls.

Using the values of FNBW given in Table 4.1, the locus of the first nulls which delimits the mainlobe is plotted in Fig. 4.1. For comparison purpose, an ellipse and a rectangle are also drawn in the same figure.

As observed from Fig. 4.1, the locus of main lobe is close to an ellipse, not a rectangle. This proves the mainlobe area can be delimited by an ellipse not a rectangle. The same delimitation can be applied to the sidelobe area

4.2.2 The Dimensions of Mainlobe and Sidelobe Areas

The one-dimension plots of IRF-SAR with $\varphi_t = 90^o$ and $\varphi_t = 0^o$ in Fig. 4.2 and 4.3 correspond to azimuth and range, respectively. Based on these plots, we can determine the dimensions of mainlobe and sidelobe areas.

From the investigation of IRF-SAR in azimuth direction, the values of HPBW and FNBW are found as follows:

Table 4.2: Values of HPBW and FNBW in azimuth direction.

HPBW	1.38×2 m	2.76 m
FNBW	3.34×2 m	6.68 m

The ratio of FNBW to HPBW in azimuth direction is therefore given by

$$\frac{\text{FNBW}}{\text{HPBW}} = \frac{6.68}{2.76} = 2.42 \tag{4.4}$$

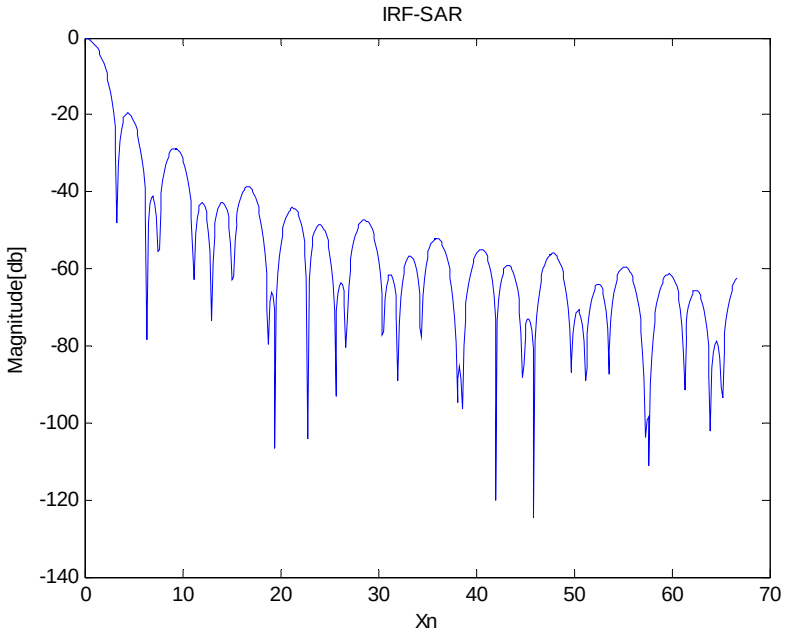

Fig 4.2: IRF-SAR in azimuth direction.

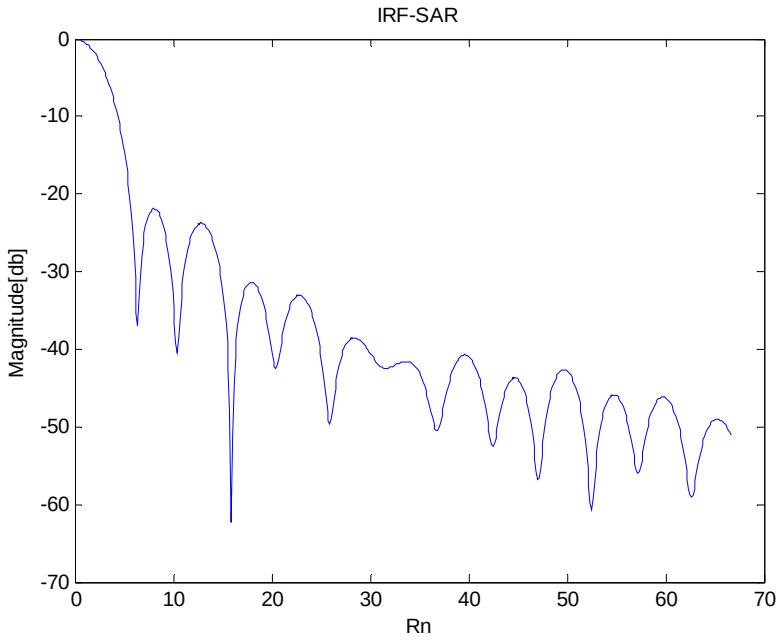

Fig 4.3: IRF-SAR in range direction.

Similarly, from investigation IRF-SAR in range direction, the value of HPBW and FNBW are given by:

Table 4.3: Values of HPBW and FNBW at range direction.

HPBW	2.6×2 m	5.2 m
FNBW	6.4×2 m	12.8 m

We can also find the ratio of FNBW to HPBW in range direction as

$$\frac{\text{FNBW}}{\text{HPBW}} = \frac{12.8}{5.2} = 2.46 \tag{4.5}$$

From these ratios, it is seen that a factor of 2.5 is sufficient to represent both the spread of the mainlobe in azimuth and range direction with respect to HPBW.

If only sidelobes above –20 dB are taken into account in the image quality assessments, a factor of 10 is reasonable to cover the spread of the sidelobes in both azimuth and range direction with respect to HPBW.

CHAPTER 5

UWB SAR Image Quality Measurements

SAR image quality measurements play an important role in the development of SAR image digital processing methods. The main objective of SAR image quality measurements is to examine the performance of a SAR system. SAR image quality measurements are based on analysis of a point target. In this chapter, UWB SAR image quality measurements are discussed.

5.1 Spatial Resolution

The spatial resolution can be defined as the distance between the points with intensities 3 dB below the maximum intensity of the peak of mainlobe. Actually these points can be considered as Half Power Beamwidth (HPBW) as they are one half of peak intensity. Spatial resolution plays an important role in SAR image quality measurements since it indicates the ability to distinguish between two targets on a SAR image. By retrieving peak intensity of a single point target, two vectors can be found which are used to determine spatial resolution both in azimuth and range. As mentioned earlier, UWB SAR deals with azimuth focusing by using large integration angles. For UWB SAR image quality measurements, different integration angles should be involved. Thus, the measurements of azimuth vector and range vector should be taken at different integration angles, for example from 5 to 70 degrees integration angles.

5.2 Differential Resolution

When it is necessary to compare between the measured results in both azimuth and range, normal resolution graphs do not give the exact results. This problem is acute when integration angles are large. In this case, differential resolution should be used for better comparison purpose. It is defined by following equations [4].

$$\Delta_{dx} = \frac{\Delta x - \Delta x_{ref}}{\Delta x_{ref}} \tag{5.1}$$

and

$$\Delta_{dr} = \frac{\Delta r - \Delta r_{ref}}{\Delta r_{ref}} \tag{5.2}$$

where Δx_{ref} and Δr_{ref} can be the theoretical azimuth and range resolutions and given by the following equations,

$$\Delta x_{ref} = \varepsilon_{x,-3} \frac{0.2211\lambda_c}{\sin\left(\frac{\phi_0}{2}\right)} \tag{5.3}$$

and

$$\Delta r_{ref} = \varepsilon_{r,-3} \frac{0.4422\lambda_c}{B_r} \tag{5.4}$$

In (5.3) and (5.4), $\varepsilon_{x,-3}$ and $\varepsilon_{r,-3}$ are HPBW broadening/narrowing factors represent the effects of the fractional bandwidth and integration angle.

5.3 Integrated Sidelobe Ratio (ISLR)

The Integrated Sidelobe Ratio (ISLR) is the ratio of the energy in the sidelobes to that contained in the mainlobe. This parameter is normally expressed in decibels [18]. With the factors to define mainlobe and sidelobe areas found in the previous chapter, ISLR of UWB SAR image can be defined as

$$\text{ISLR}|_{\text{dB}} = 10\log\left|\oiint_{(10\Delta x,10\Delta r)} |I|dA - \oiint_{(2.5\Delta x,2.5\Delta r)} |I|dA\right| - 10\log\left|\oiint_{(2.5\Delta x,2.5\Delta r)} |I|dA\right| \tag{5.5}$$

where I is the intensity and dA is the derivative of the area.

5.4 Peak Sidelobe Ratio (PSLR)

The Peak Sidelobe Ratio (PSLR) is the ratio between the returned signal of the mainlobe and that of the first sidelobe of the point signal. This parameter is also expressed in decibels.

$$\text{ISLR}|_{\text{dB}} = 10\log|I_s| - 10\log|I_M| \tag{5.6}$$

where I_S is the peak intensity of the sidelobe area and I_M is the peak intensity of the mainlobe area.

CHAPTER 6

UWB SAR Image Quality Measurement Results

In this chapter, we measure the quality of an UWB SAR image based on the assessments presented in Chapter 5. They are spatial resolution, differential resolution, Integrated Sidelobe Ratio (ISLR), and Peak Sidelobe Ratio (PSLR). The UWB SAR image is formed with the simulated data of the UWB low frequency SAR system CARABAS-II. Its main parameters are summarized in Table 6.1.

Table 6.1: CARABAS-II parameters

Parameter	**Value**
Highest frequency f_{max}	80 MHz
Lowest frequency f_{min}	20 MHz
Speed of aircraft v_{pl}	129 m/s
Flight altitude h	2500 m
Aperture step Δ_L	0.9375 m
Minimum Range to the aim point r_0	7000 m
Integration angle α	$5^\circ - 70^\circ$

6.1 Spatial resolution and differential resolution measurements

For resolution and differential resolution measurements, two vectors in azimuth and range directions are extracted from the retrieved peak intensity of a single point target. Since UWB SAR systems are always involved with large integration angles to handle azimuth focusing, resolution and differential resolution should be measured at different integration angle. Integration angles from 5 degrees to 70 degrees are used in the following measurements. Fig. 6.1.a shows an example of UWB SAR image reconstructed from the simulated CARABAS-II data with an integration angle of 65 degrees. The extractions of the azimuth and range vectors from the retrieved peak intensity of the single point target are given in Fig. 6.1.b and 6.1.c, respectively. For determining azimuth resolution from Fig. 6.1.c, we take the distance between the points with intensities 3 dB below the maximum intensity of the mainlobe peak. The spatial resolution in azimuth is 2.34 m. Similarly, the range resolution is found from Fig. 6.1.b to be 2.31 m.

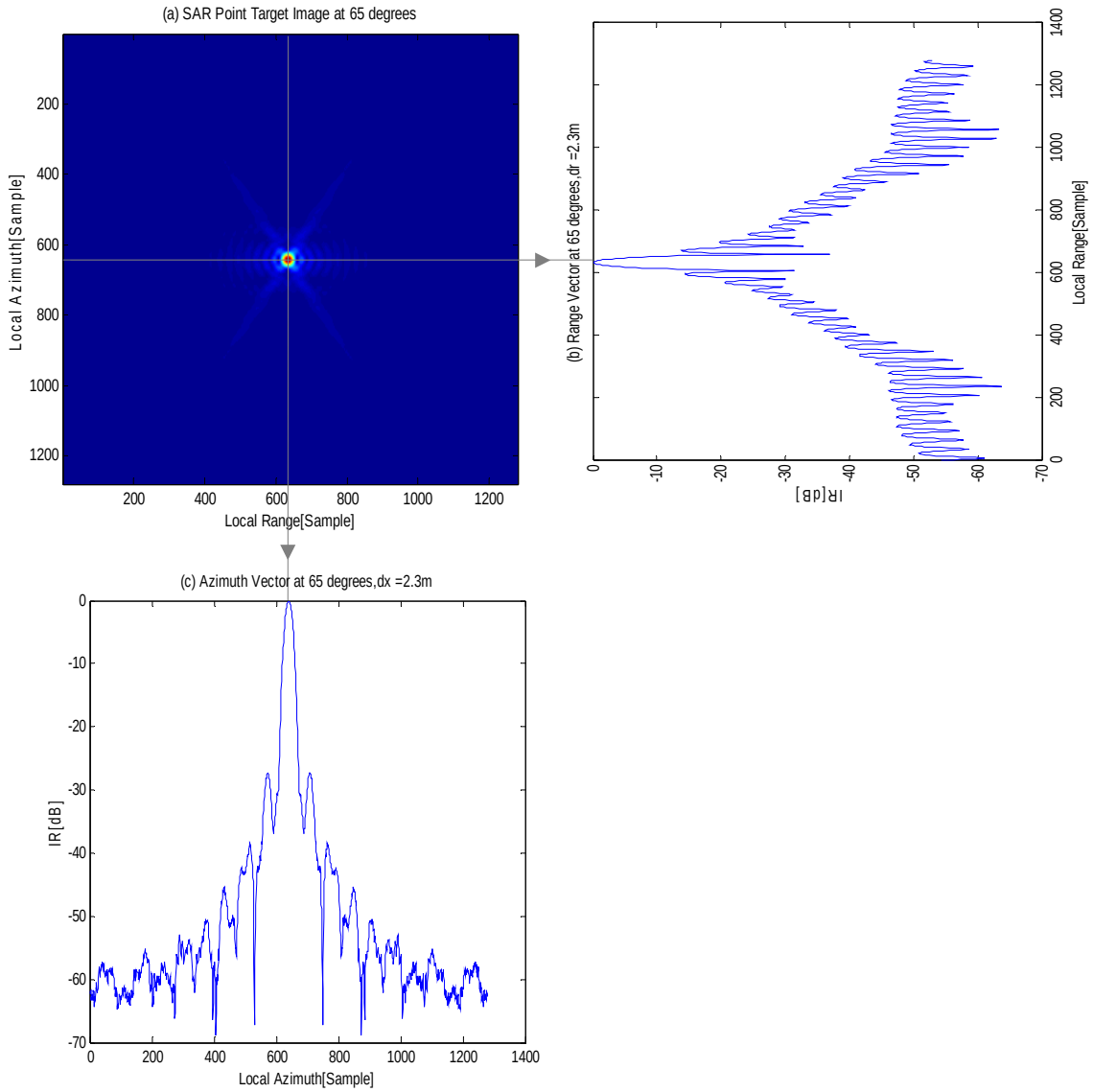

Fig. 6.1: (a) A point target is imaged by an UWB SAR system with an integration angle of 65 degrees, (b) The extracted range vector from the peak, (c) The extracted azimuth vector from the peak.

The same procedure is applied to the UWB SAR image reconstructed from the simulated CARABAS-II data with other integration angles in order to find spatial resolutions at different integration angle. The measured results are summarized in Table 6.2. From the table 6.2 we can see that the azimuth resolution at 5 degrees is only 29.44 m and with increasing integration angle the azimuth resolution becomes better. The finest resolution in azimuth in the tested angle range is achieved at 70 degrees which is 2.18 m. The range resolutions are almost the same at different integration angles. We get almost equal spatial resolutions in azimuth and range at 65 degrees.

Table 6.2: Spatial resolutions in range and azimuth measured at different integration angles.

Integration angle α (degree)	**Range resolution Δr (m)**	**Azimuth resolution Δx (m)**
5	2.20	29.44
10	2.22	14.62
15	2.22	9.86
20	2.22	7.42
25	2.23	5.92
30	2.24	4.95
35	2.25	4.26
40	2.26	3.72
45	2.26	3.32
50	2.28	3.00
55	2.29	2.74
60	2.31	2.52
65	2.31	2.34
70	2.32	2.18

We can also plot the values given in Table 6.2 to get a better illustration of the resolution behavior in range and azimuth. Fig. 6.2 shows the plot the measured results of the spatial resolutions in range and azimuth.

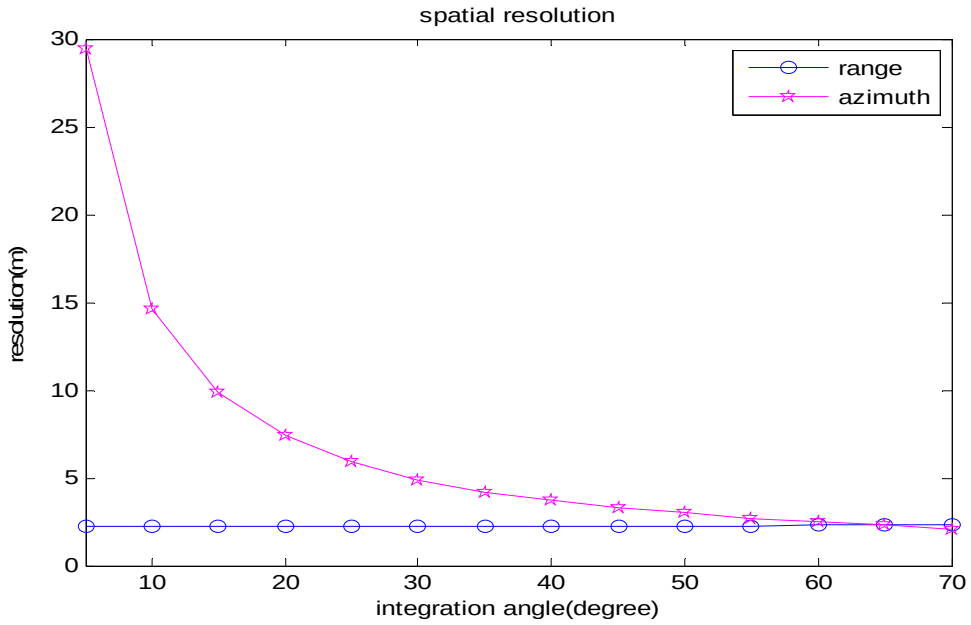

Fig. 6.2: Plot of the spatial resolutions measurements

Table 6.3: Differential resolutions in range and azimuth calculated at different integration angles.

Integration angle α (degree)	**Differential resolution in range Δ_{dr} (%)**	**Differential resolution in azimuth Δ_{dx} (%)**
5	0.49	3.24
10	0.41	4.03
15	0.41	3.00
20	0.41	2.87
25	0.86	2.77
30	1.31	3.32
35	1.76	3.66
40	2.22	4.07
45	2.22	4.24
50	3.12	4.43
55	3.57	4.63
60	4.47	4.90
65	4.47	5.26
70	4.92	5.62

From Fig 6.2, we can see that an increase in azimuth resolution is proportional to an increase in integration angle. The azimuth resolution obtained at 70 degrees is higher approximately 15 times than one at 5 degrees, whereas the range resolution is always high and almost a constant at different integration angles. Assuming that we need to evaluate the performance of this simulated SAR system based on the spatial resolutions or to compare the performances of different SAR systems. Such evaluation or comparison seems to be difficult for azimuth resolutions at wide integration angles, especially above 60 degrees, and range resolutions. In these cases, differential resolutions are good measurements for evaluation or comparison purposes. In the following example, a comparison between the measured spatial resolutions $\Delta x$and Δr given in Table 6.2 and the theoretical resolutions Δx_{ref} and Δr_{ref} given in (5.3) and (5.4) is presented.

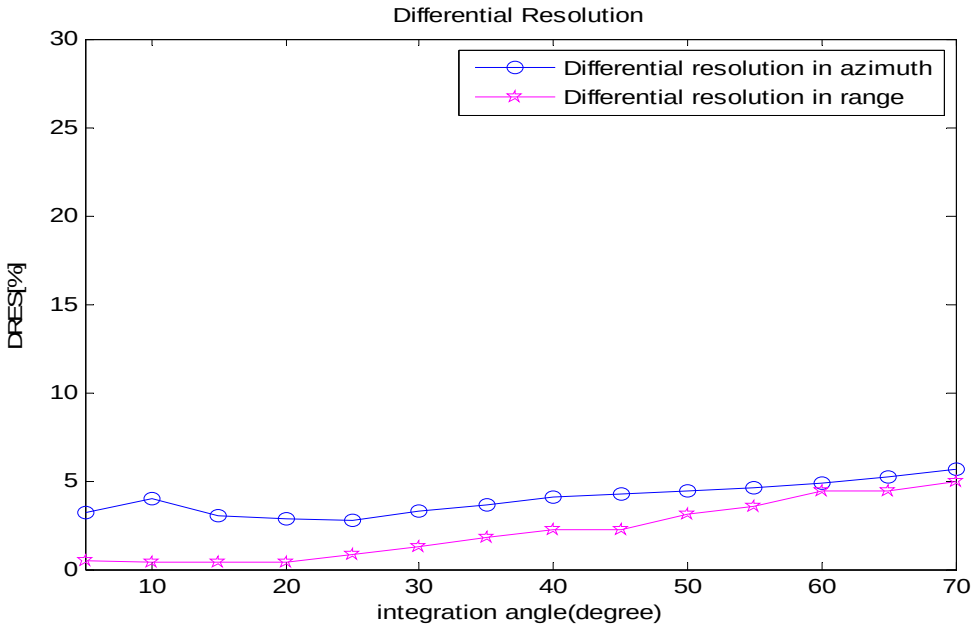

Fig 6.3: Plot of the differential resolution calculations.

For the illustration purpose, we select $\varepsilon_{x,-3}$=1 and $\varepsilon_{r,-3} = 1$ which are the approximate HPBW broadening/narrowing factors represent the effects of the fractional bandwidth and integration angle. The differential resolutions in azimuth and range, for example at 65 degrees, are calculated as follows:

$$\Delta_{dx}= \frac{2.34 - 2.47}{2.47} \times 100\% = 5.26\%$$

$$\Delta_{dr}= \frac{2.31 - 2.21}{2.21} \times 100\% = 4.47\%$$

Table 6.3 shows the differential resolutions in range and azimuth at different integration angles. The calculated results are also plotted in Fig. 6.3.

From the Table 6.3 we see that the maximum differential resolution is only 5%. On one hand, we can conclude that the performance of the simulated SAR system is quite good in terms of SAR image quality assessments. On the other hand, we can say that the resolution equations (5.3) and (5.4) are accurate. From the Fig. 6.3 we see that at larger integration angles the differential resolutions in azimuth and range still allow us to evaluate the performance of a SAR system and compare between SAR systems. Such tasks are not possible if only based in Fig. 6.2.

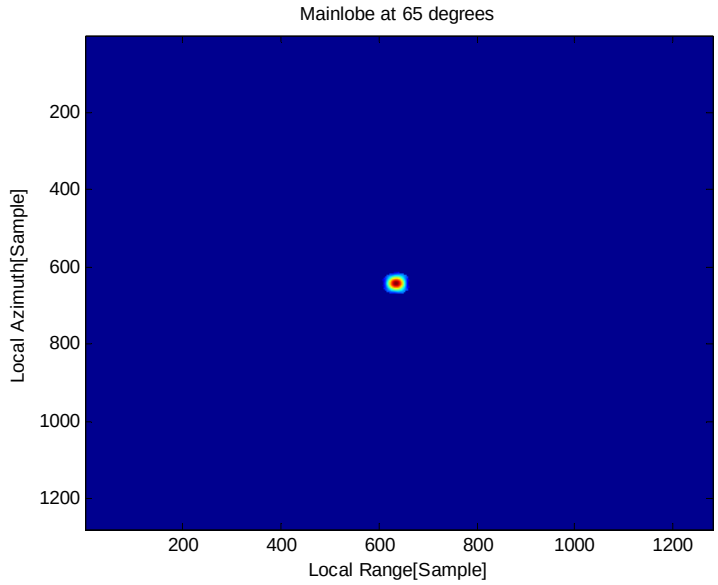

Fig. 6.4: Mainlobe area delimitation at 65 degrees.

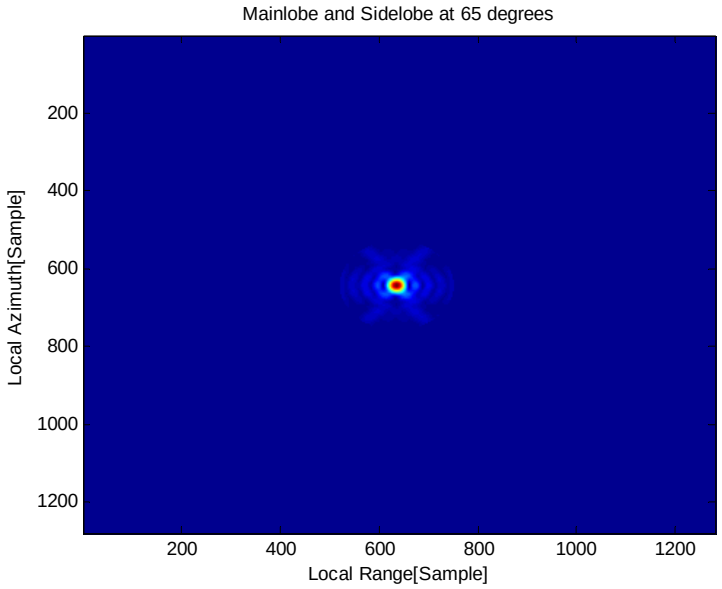

Fig. 6.5: Mainlobe plus sidelobe area delimitation at 65 degrees.

6.2 ISLR and PSLR measurements

For ISLR and PSLR measurements, we delimit the mainlobe and sidelobe area of a SAR image of a point target by ellipses. The mainlobes is defined by a small elliptical area whereas the mainlobe plus sidelobe area is limited by a bigger elliptic area. The dimensions of these ellipses are given by $(2.5\Delta_a, 2.5\Delta_r)$ and $(10\Delta_a, 10\Delta_r)$ as defined in Chapter 4.

Table 6.4: ISLR and PSLR at different integration angles.

Integration angle α (degree)	**ISLR (dB)**	**PSLR (dB)**
5	-6.96	-13.13
10	-7.01	-13.29
15	-7.06	-13.55
20	-7.06	-13.56
25	-7.05	-13.65
30	-7.19	-13.82
35	-7.32	-14.03
40	-7.28	-14.06
45	-7.34	-14.14
50	-7.42	-14.36
55	-7.42	-14.49
60	-7.49	-14.56
65	-7.50	-14.73
70	-7.67	-15

Fig. 6.4 and 6.5 depict the mainlobe and the mainlobe plus sidelobe areas of a SAR image of a point target at 65 degrees by using the elliptic areas $(2.5\Delta_a, 2.5\Delta_r)$ and $(10\Delta_a, 10\Delta_r)$, respectively. Applying (5.5) and (5.6), we can estimate ISLR and PSLR in dB scale as

$$\text{ISLR}|_{\text{dB}} = 10\log\left|\oiint_{(10\Delta x,10\Delta r)} |I|dA - \oiint_{(2.5\Delta x,2.5\Delta r)} |I|dA\right| - 10\log\left|\oiint_{(2.5\Delta x,2.5\Delta r)} |I|dA\right| = 7.5 \text{ dB}$$

and

$$\text{PSLR}|_{\text{dB}} = 10\log|I_s| - 10\log|I_M| = -14.73 \text{ dB}$$

The same measurements are employed at different angle and the measurement results are summarized in Table 6.4. These values are also plotted in Fig. 6.6 for more illustrative.

From Fig. 6.6, we can see that both ISLR and PSLR slightly decrease with an increase of the integration angle. For example, the highest value of ISLR achieved at 5 degrees is –6.96 dB whereas the lowest value of ISLR is found at 70 degrees which is –7.67 dB. Also, for PSLR measurements, we get the highest value –13.13 dB at 5 degrees and the lowest value is –15 dB at 70 degrees.

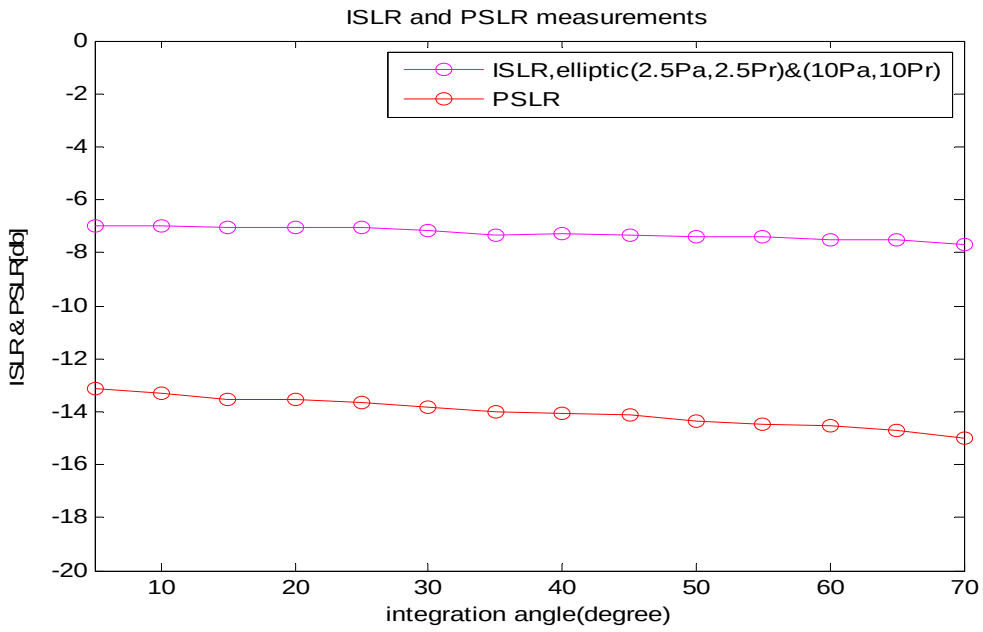

Fig 6.6: ISLR and PSLR at different integration angles.

In UWB SAR, integration angle is proportional to azimuth resolution while inversely proportional to mainlobe and sidelobe area. At a large integration, the azimuth resolution can be high but the mainlobe and sidelobe areas are small. Thus, ISLR and PSLR do not change much while resolution in azimuth increases significantly. This explains why the ISLR and PSLR are almost constant at different integration angles.

CHAPTER 7

Conclusions and Recommendations

In this thesis work, a definition of UWB SAR image quality measurements is presented and the measurements for the UWB SAR image are performed. The most crucial UWB SAR image quality assessments are spatial resolution, differential resolution, ISLR and PSLR. Due to the characteristics of UWB SAR, these measurements are proposed to be performed at different angles. We manage to find the broadening factors of the mainlobe and sidelobe areas and prove that the locus of the first nulls of the mainlobe is elliptical not rectangular. For these tasks, we use a newly defined IRF-SAR instead of the currently used *sinc* function. Also, a factor of 2.5 is shown to be sufficient to represent the spreading of the mainlobe in both azimuth and range directions.

In this study, the simulated CARABAS-II data is employed. For UWB SAR image formation, the time-domain algorithm GBP is chosen because it generates minimum phase error. Based on the SAR images of a point target formed at different integration angles, the finest resolution is achieved at large integration angles. But at large integration angles it is difficult to compare or evaluate the performance of the UWB SAR systems, so differential resolution is used. We see that the differential resolution shows the better comparison or evaluation performance of a SAR system. Also the lowest ISLR and PSLR values are obtained at wide integration angles. So it can be concluded that the better image quality performance of a UWB SAR is achieved with large fractional bandwidth and wide integration angles.

References

[1] M. I. Skolnik, “Radar handbook”, MCGraw-Hill, New York, 1970.

[2] Dr. P. Berens, “Introduction to synthetic aperture radar”, Research and Establishment for Applied Science (FGAN), Watchberg, Germany, 2006.

[3] S. Noorizadeh, “An introduction to synthetic aperture radar solution”, the final project report of the Introduction to Radar and Electromagnetic Remote Sensing (ECE 4390), Georgia Institute of Technology, Atlanta, Georgia, 2010.

[4] V. T. Vu, T. K. Sjögren, M. I. Pettersson, A. Gustavsson, “Definition on SAR image quality measurements for UWB SAR”, in Proc. SPIE Image and Signal Processing for Remote Sensing XIV, vol.7109, Cardiff, UK, September 2008, pp. 7109A1 – 7109A9 .

[5] V. T. Vu, “Practical consideration on ultrawideband synthetic aperture radar data processing”, Licentiate Dissertation Series, Blekinge Institute of Technology, Sweden, November 2009.

[6] R. T. Lord, “Radio Frequency Interference Suppression applied to Synthetic Aperture Radar Data”, XXVIIIth General Assembly of International Union of Radio Science, URSI 2005, New Delhi, India, October 2005.

[7] Y. K. Chan, and V. C. Koo, “An introduction to synthetic aperture radar (SAR)”, Progress in Electromagnetic Research B, vol. 2, pp. 27 – 60, 2008.

[8] J. C. Curlander, and R. N. McDounough, “Synthetic aperture radar, systems and signal processing”, John Wiley and Sons, New York, 1991.

[9] A. K. Badiambile, “Synthetic aperture radar processing”, African Institute for Mathematical Sciences (AIMS), South Africa, May 2008.

[10] G. Barrie, “Ultra-wideband synthetic aperture, data and image processing”, Defence research and Development, Canada-Ottawa, 2003.

[11] http:// www.grss-ieee.org/wp-content/uploads/2010/06/Radar_Interferometry_Part1.pdf

[12] D. Wong and L. Carin, “Analysis and processing of ultrawide-band SAR imagery for buried landmine detection,” IEEE Transactions on Antennas and Propagation, vol. 46, no. 11, pp. 1747-1748, November 1998.

[13] http:// www.cm.nctu.edu.tw/~IEEEITComSoc/.../Ultra%20Wide%20Band.pdf

[14] J. R. Bennett and I. G. Cumming, ”Digital processor for the production of Seasat synthetic aperture radar imagery,” in Proc. International Conference On Seasat-SAR Processor, Frascati, Italy, Dec. 1979, ESA-SP-154.

[15] R K. Raney, fellow, IEEE, H. Runge, R. Balmer, I. G.Cunning and F. H.Wong, "Precision SAR processing using chirp scaling, " IEEE Transactions on Geoscience and Remote Sensing, vol. 32, no. 4, pp. 786-799, 1994.

[16] B. Cordes, "Parallel Backprojection: A case study in high performance reconfigurable computing," Graduate School of Engineering, Northeastern University, Boston, Massachusetts, April 2008.

[17] V. T. Vu, T. K. Sjögren, M. I. Pettersson, and H. Hellsten, "An impulse response function for evaluation of ultrawideband SAR imaging", IEEE Trans. Signal Processing, vol. 58, no.7, pp. 3927-3932, July 2010.

[18] *A. Martínez, and J. L. Marchand*, "SAR image quality assessment", Revista de Teledeteccion, 1993.